Sensing form - finger gaiting as key to tactile object exploration: A data glove analysis of a prototypical daily task

Werner Krammer (werner.krammer@kssg.ch)
Inselspital Universitatsspital Bern https://orcid.org/0000-0003-2464-4911
John H. Missimer
Paul Scherrer Institut
Simon Habegger
Inselspital Universitatsspital Bern
Manuela Pastore-Wapp
Inselspital Universitatsspital Bern
Roland Wiest
Inselspital Universitatsspital Bern
Bruno J. Weder
Inselspital Universitatsspital Bern

Research

Keywords: object in-hand manipulation, precise handling, finger gaiting, finger synchrony, time series, principal component analysis, graph analysis

Posted Date: January 17th, 2020

DOI: https://doi.org/10.21203/rs.2.21200/v1

Version of Record: A version of this preprint was published on October 8th, 2020. See the published version at https://doi.org/10.1186/s12984-020-00755-6.

Abstract

Background

Motor hand skill with associated dexterity is an important facility in meeting the challenges of daily activity and an important resource post-stroke. In this context, the present study investigated the finger movements of right-handed subjects during tactile manipulation of a cuboid, a prototypical component of tactile exploration.

Methods

For both hands of 22 subjects, we acquired the time series of consecutive multifinger cuboid manipulations using a digital data glove consisting of 29 sensors. Of these, 16 recorded the bending of metacarpo-phalangeal (MCP) and proximal interphalangeal (PIP) joints of the fingers, MCP and interphalangeal IP joints of the thumb, palm arch and carpo-metacarpal (CMC) joint of the thumb, and abduction between fingers.

Results

Using principle component analysis we decomposed the short action into motor patterns related to successive manipulations of the cuboid. The fraction of variance described by the principal components indicated that three components described the salient features of the single motor acts for each hand. Striking in the finger patterns was the prominent and varying roles of the MCP and PIP joints of the fingers, and the CMC joint of the thumb. An important aspect of the three components was their representation of distinct finger configurations within the same motor act. Principal component and graph theory analysis confirmed modular, functionally synchronous action of the involved joints. The computation of finger trajectories in one subject illustrated the workspace of the task, which differed for the right and left hands.

Conclusion

The study substantiates finger gaiting, described until now only in artificial systems, as the principal mechanism underlying this prototypical task, which is ubiquitous in daily object shape recognition.

Background

Motor hand skill is an important facility in meeting the challenges of daily activity and its loss a critical consequence of stroke [1, 2]. Manual dexterity relies on motor control exerted during active touch, which is essential to tactile object manipulation and exploration [3]. The relationship between tactile object manipulation and dexterity is evident in proposed definitions of the latter: "(The) process in manipulating an object from one grasp configuration to another" [4] or "(The) capability of changing the position and orientation of the manipulated object from a given reference configuration to a different one, arbitrarily chosen within the hand workspace" [5]. Motor hand skill depends on sensory guidance via proprioceptive

control afferents, as has been shown in corticokinematic coherence studies of active and passive finger movements, i.e. studies of coupling between magnetoencephalographic signals and hand kinematics. It involves mainly the primary sensori-motor (SM1) cortex [6]. Also during the manipulation involved in tactile object recognition, fingers move in a proprioceptive motor space [7]. The proprioceptive motor space occupied by thumb and finger trajectories, linked by the motor, tactile and kinesthetic sensory systems of the hand, utilizes only a small percentage of the workspace available to the involved joints [8].

Roland and Mortensen [9] developed a theoretical model of human somatosensory exploration of kinesthesia, macrogeometry, size and shape which describes the input-output relationships of tactile exploration. Using their fully quantified macrogeometrical stimuli, i.e. a set of parallelepipeds and spheres of identical volume representing non-real objects, we and others have verified three modes of exploration in extended actions of digital object exploration [10, 11]. These modes consist of coordinated dynamic digital movements of the fingers (mainly thumb, index and middle finger), including intervals of rotating and encompassing the object with the three middle fingers. As measured by video-monitoring, the dynamic movement of the thumb consumed the most time. This mode of exploration disappeared in over-learned pure motor sequences at high frequency [12]. We have confirmed the dominance of dynamic thumb movements in behavioral and fMRI activation studies [10, 13].

Investigations in two fMRI studies of finger movements analogous to those underlying tactile exploration but without cognitive load revealed two patterns of cerebral activation during elementary tactile manipulation: a dominant pattern of motor control involving the primary motor and sensory cortex (SM1) as well as the premotor cortex, and a subdominant pattern reflecting less voluntary control [11]. In a recent study of healthy elderly subjects manipulating cuboids, we replicated these findings while imposing a dynamic grasp frequency of 1 Hz, consistent with the frequencies of sensory guided actions in humans [14].

In our paradigm the hand action consisted of smoothly changing finger configurations in which the opposed thumb and multiple fingers surrounded the objects, sliding over their surface. This sequence of manipulations has been described in artificial systems as finger gaiting [15, 16]. In a neurobiological perspective a series of changing elementary precision grip or grasp configurations conform to precision handling, a concept developed by Landsmeer [17]. The hallmark of elementary precision grip is the opposition of thumb and single fingers whereas power grip is characterized by opposition of thumb and all fingers [18]. In contrast finger gaiting is a task requiring multiple independently controlled contacts, designated virtual fingers, to optimize the object orientation during one motor act [19]. Landsmeer distinguished the static and dynamic phases of a manipulation in which properly placed finger tips and opposed thumb hold the object, after which they move to perform the manipulation or handling. Precise handling enables the subject to perform intrinsic hand movements of the object without moving the arm [17, 20].

In recent years finger adaptation to objects of different size and shape during reach-to-grasp have been tested using both glove data and finger contact positions [21–23]. Here, we investigate pure manipulation

of a cuboid using a digital data glove equipped with 29 sensors. Our goal was the study in a multidigit approach of the spatial and temporal features of characteristic finger movement patterns for right and left hand of right-handed subjects performing a prototypical task underlying tactile object exploration. In contrast to earlier investigations of reaching-to-grasp mentioned above, the motor acts required by the task consisted only of in-hand prehensile finger movements. Unlike tactile exploration, the task did not involve a cognitive element; the cuboid had almost identical spatial dimensions and physical properties. In the study, twenty-two normal subjects manipulated repeatedly a cuboid at a frequency of 1 Hz, as instructed previously via a video. The time series of the 19 sensors observed to be associated with dynamic digital movements were subjected to a principal component analysis (PCA) for all subjects and sessions, yielding common sensor and temporal patterns. Composed of temporal and spatial features, these patterns represent the dynamical digital movements constituting grasp configurations. The spatial patterns were classified using cluster analysis to assure homogeneity of the components. Graph and frequency analysis of individual finger movements yielded complementary aspects of the manipulation. The finger movements of a single subject in 3D space illustrated the dynamics of the manipulation. We hypothesized that the short motor actions of prehensile in-hand manipulation performed during the task may be decomposed into single motor acts of opposing thumb and finger configurations that underlie tactual exploration of an object. The description of the patterns in healthy subjects is intended to provide a standard of comparison for a study of recovery after stroke.

Subjects And Methods

Subjects

Twenty-two healthy right-handed subjects, 10 males and 12 females ranging in age between 42 and 84 years with a median age of 59, were included in the study. The handedness score according to the Edinburgh Handedness Questionnaire [24] ranged between 50 and 100 with median 100. The subjects had no prior history of psychological disorders, achieved normal Mini-Mental State Examination (MMSE) scores, and exhibited no pathological findings in the T1-MRI brain scans. Demographic data are shown in Table 1. The study received ethical approval from the Kantonale Ethikkommission Bern (KEK), 3010 Bern, Switzerland. Prior to the study all participants gave written informed consent before enrolment, according to the Declaration of Helsinki [25].

Table 1
Demographic subject data.

ID	gender	age (years)	LQ	MMSE
1	m	74	90	27
2	f	73	60	29
3	m	42	100	30
4	f	48	60	29
5	f	65	50	27
6	f	71	100	28
7	m	47	100	30
8	f	52	100	30
9	f	59	90	29
10	m	53	100	26
11	m	54	70	29
12	f	47	100	30
13	f	51	100	29
14	f	56	100	29
15	f	59	80	30
16	f	69	100	28
17	m	84	100	28
18	m	83	80	29
19	f	69	90	29
20	m	75	100	28
21	m	68	100	27
22	m	71	100	29
N or Median	10 m / 12 f	62	100	29
Range		42–84	50–100	26–30

(m, male; f, female; LQ, laterality quotient; MMSE, Mini-Mental State Examination)

Sensori-motor assessment

Sensori-motor function was assessed with five measurements for both left and right hands: (1) Power grip was calculated from the average of three power grips using a Jamar hydraulic hand dynamometer [26]; (2) Averaged over three trials, precision grip was measured while applying pinch force between thumb and index finger at the groove of a Jamar hydraulic pinch gauge [26]; (3) Motor hand skill of each hand was determined using one of the seven timed subtests comprising the Jebsen-Taylor Test (JTT), namely, “Picking Small Objects” (PSO) in which subjects grasp six small common objects (two each of paper clips, bottle caps and coins) and drop them into an empty can; (4) Two-point discrimination (2PD) was measured using a graded caliper [2-point Discriminator, Medwork Instruments, Vancouver, Canada] on the index fingertip [27]; and (5) tactile object recognition (TOR) was tested using a standardized protocol employing 30 everyday objects as previously described [28]. The assessments were intended to confirm normal sensori-motor abilities in the subjects; they were not incorporated in analyses of the task.

Data glove instrumentation and calibration

We employed the VMG 30™ data glove from Virtual Motion Labs [Virtual Motion Labs, LLC., 3010 LBJ Freeway, Dallas, Texas 75234 (see www.virtualmotionlabs.com)]. The glove is equipped with 29 sensors of which 16 are bend sensors less than 0.35 mm in thickness. Two finger bend sensors per finger for measure the movement extent in the metacarpo-phalangeal (MCP) and proximal interphalangeal (IP) joints, and two finger bend sensors at the thumb measure movement extent in the MCP and IP joints. Four sensors between the fingers measure abduction. One palm arch sensor detects spatial configuration related to the proximal and distal transverse arch of the hand described by Hertling and Kessler [29]. One thumb cross sensor detects the complex movement of the thumb during finger opposition at carpo-metacarpal (CMC) joint. Five sensors situated at the finger tips measure pressure and eight sensors measure hand and wrist orientation (Figs. 1A, 1B). Calibration of the data glove consisted of seven calibration stages: (1) maximal simultaneous flexion and extension of all fingers and thumb simultaneously at a frequency of 1 Hz, (2) alternating maximum adduction and abduction of all fingers at a frequency of 1 Hz, (3) maximal transaxial extension of the thumb (including an associated inward rotation) related to CMC joint to the little finger, and maximal flexion of MCP and PIP joints in all fingers. Finally, one opposing movement of the thumb to the index (4), middle (5), ring (6) and little (7) finger pad, forming an “O” between the thumb and fingers were carried out. Bend sensors were calibrated between a value of 1000 (flexion in the MCP and PIP joints, adduction of fingers, transaxial extension of the thumb and forming the palm arch) and of 0 (maximal extension in the finger joints, abduction of fingers, resting position of the palm arch and CMC joint of thumb). Finger pressure sensors were calibrated between a value of 1000 for no pressure and 0 for maximum pressure.

Task performance

The sensori-motor task consisted of regular single motor acts at a frequency of 1 Hz in which the opposed thumb and fingers of one hand surround the cuboid in a continuous and regular action. The almost identical axes of the cuboid avoid the distraction and reorientation induced by significantly different axes. Consecutive steps of the motor act as displayed in the instruction video are depicted in

Fig. 1C, which shows successive phases of the thumb and finger trajectories. Each phase begins with a transaxial movement of the thumb versus the ring finger. During the concerted action of thumb and fingers in the workspace, the thumb exerts tangential forces that produce a marked rotation of the object, anticlockwise in the right hand, and clockwise in the left. In the terminology of Bullock et al. [30], 1) the action is prehensile, 2) the stabilizing fingers change continuously during one motor act, 3) the cuboid moves, guided by the tip of the thumb, relative to the contact points of the virtual fingers [19], 4) thumb and fingers move relative to the reference frame defined by the hand base, and 5) the motor sequence of fingers and thumb is repeated at the given frequency.

The cuboid was made of granite with a weight of 29.9 gram and side lengths of 22.54 × 22.54 × 22.57 millimeters resulting in a total volume of 11.5 cm^3, comparable with those of the aluminum cube used in [14]. The density of 2.6 g/cm^3 was also comparable to that of aluminum, 2.75 g/cm^3. A video was filmed to instruct the subjects how to perform the task. This video consisted of three, 20 seconds long, consecutive segments: (1) fixation, (2) observation, (3) active manipulation, each announced by written instruction on a blank white screen for 4 seconds. “Fixation” showed a hand holding the cube; “Observation” showed the same hand manipulating the cuboid at the prescribed 1 Hz; and upon “Active manipulation” the subjects were given the cube by the study physician and requested to manipulate the cube at the required speed as shown in the video sequence displayed during the segment “Observation” on the screen. A right hand was shown for the right hand sensori-motor task and a left hand for the left hand sensori-motor task. The 3 segments were repeated six times showing 3 male and 3 female hands and resulting in a total video length of 7.2 minutes. In- house software recorded the sensor data only during the 20 seconds of active manipulation.

During task performance, subjects were seated at a desk on which was placed a computer screen with their hands supine on the desktop. The motor task was explained by the study physician, and subjects requested to manipulate the cuboid with the left and right hand without the data glove for about 10 seconds as shown by the physician. This procedure ensured that subjects understood the task. Then the calibrated data glove was put on the non-dominant left hand of the subject and checked for fit by the physician. The video was started when the subject's hand was relaxed on the table top. When the instruction “Active manipulation” appeared on the screen, the physician placed the cuboid in the subject's hand; after completion of the segment, the cuboid was removed. The glove calibration procedure required a break of about 2 minutes between acquisitions with the left and right hand.

Data sampling

Data were acquired with software programmed in house and based on the Software Development Kit provided by Virtual Motion Labs. Pre-study testing of the signals produced by the task indicated that they could be most efficiently encoded at a frequency of 50 Hz, implying time frames of 20 msec. This frequency appears sufficient in reference to the published critical thresholds of about 20 Hz for steady visual perception and 10 Hz for visual parsing [31]. One action of consecutive manipulations is denoted a run and consisted of 1000 time frames. In order to i) exclude irregularities as the subject adjusted to

prescribed frequency of manipulation observed in the instruction video and ii) to impose a standard number for subsequent analysis, only the last 800 time frames, i.e 16 sec, of each run were analysed.

Data analysis

All nineteen sensor time courses of each run and subject reflecting prehensile in-hand manipulation were submitted to principal component analysis (PCA, see results): all ten finger bend sensors, all four ab/adduction sensors, and the two sensors describing the deformation of the palm (palm arch, thumb cross); additionally three pressure sensors at the finger tips 1 to 3 mainly involved in the manipulation task.

Separate analyses were performed for each hand. PCA was performed using in house software written in Matlab [The Mathworks, Inc., Natick, MA] based on the algorithm described by Alexander and Moeller [32]. The sensor amplitudes for each sensor in the 800 time frames were entered in a matrix. The rows corresponded to the 800 time frames and columns to the 19 relevant sensors of a run. PCA is applied to a residual matrix. To compute this matrix, (i) the mean of sensor amplitudes for each time frame and (ii) the mean amplitude for each sensor of all time frames are subtracted from each matrix element, and (iii) the grand mean of sensor amplitudes in the original matrices added. The row, column and grand means of the resulting residual matrices vanish. Using the singular value decomposition implemented in Matlab, the residual matrix was then decomposed into 19 principal components (PC). Each PC consisted of a sensor expression pattern, a time course and an eigenvalue. The sensor expression coefficients describe the amount each sensor contributes to the component. The time course represents the variation of the component with time and the eigenvalue characterizes the fraction of variance described by each component. The sensor expression coefficients and time courses of a PC are orthonormal and range between − 1 and 1; the orthogonality reflects the lack of statistical correlation among the principal components.

Preliminary analysis showed that the first three PCs of each run and subject explained about 75% of the variance, a number consistent with the Guttman-Kaiser criteria for salient PC [33]. Further analysis was therefore restricted to these first three PCs.

Spatial sensor patterns

Statistical analysis of the sensor expression coefficients must take into account the indeterminacy of the signs associated with multilinear models such as PCA [34] i.e. two different sets of coefficients expressing the same pattern might differ only in the signs of the sensor contributions. Before analysis of the subject cohort, alignment of the expression coefficients is therefore necessary. Alignment was performed in two stages. First, pairwise correlations of the expression coefficients were computed for the six runs of each subject and PC and the signs adjusted to yield the highest positive correlation. Second, the realigned expression coefficients of the 22 subjects were submitted to a second pairwise correlation analysis using the most favorable alignment among subjects, i.e. highest correlation, as a standard to determine the relative signs among subjects. Based on the two steps of calibration procedure and preliminary analyses of the principal components, we then assigned a positive sign to highest

correlations as reflecting increased bending of the thumb cross, MCP and/or PIP finger sensors. Thus, sensors yielding prominent positive signals indicate bending movements or pressure synchronous with the selected finger sensors. Sensors yielding prominent negative signals indicate that the bending or pressure are out of phase compared to sensors exhibiting a positive sign, but with the same time course.

In order to assure the homogeneity of the component expression coefficients for the complete cohort, k-means clustering was applied to the 3 PCs in all 132 runs and subjects, i.e. 6 runs for the 22 subjects. An iterative method for partitioning data, k-mean clustering yields mutually exclusive clusters after determining their central members. Therefore, each expression coefficient is assigned to a cluster and its distance to the central member, denoted centroid, is computed. Homogeneity of the coefficients would imply that the clusters should correspond to the rank of the PC in explaining the variance of the coefficients, i.e. the PCs explaining the greatest variance would compose one cluster, the PCs explaining the second greatest variance a second cluster, and so on. To be consistent with the number of PCs considered in each run, we limited the number of clusters to three. We implemented the clustering using the program k-mean of Matlab. The distance between centroid and cluster member was computed using the option “correlation”, as suggested by the alignment procedure.

In order to evaluate the salience of the individual sensors in the task, medians, percentiles and confidence levels for the correctly identified component expression coefficients were computed and compared with the centroid. Correctly identified coefficients are those for which the PC is labeled as belonging to its corresponding cluster, i.e. the dominant PC, PC1, of a particular run and subject is correctly identified if it is labeled as belonging to the cluster characterized by a predominance of PC1's. To confirm the salience of individual sensors, a Kruskal-Wallis test of the sensor distributions, corrected for multiple comparisons of ranks, was performed using the Matlab programs, kruskalwallis and post-hoc multicompare.

Temporal sensor patterns

To investigate the temporal properties of the PC clusters, frequency spectral analysis was applied to the time courses of correctly identified PCs. In addition, time delays between PCs for each run and subject were computed using the Matlab program finddelay. The sampling frequency of 50 Hz determined the maximum delay of 25 frames in the program, corresponding to one half of a sampling cycle.

In addition to the PCA, the frequencies and time delays among twelve individual sensors for all runs and subjects correctly assigned to Cluster 1 for both hands were also analysed; the sensors comprised the ten finger bends (i.e. related to MCP and PIP joints) and thumb cross (i.e. related to CMC joint and palm arch sensors). To reduce the noise in the time courses due to the discontinuous signal, the time courses were first filtered using a finite impulse response (FIR) filter with low pass cutoff frequency of 10 Hz. To achieve similar gain levels, they were normalized such that the magnitude of the maximum amplitude was unity. This preprocessing was implemented using the Signal Processing Toolbox of Matlab. The frequencies were determined by the time difference between signal maxima using the Matlab program findpeaks, Matlab. The time differences between minima and null positions confirmed the frequencies. The delays were limited to maximum delay of 25 frames as above.

Graph analysis of selected sensor time series

Using the same time series of the 12 MCP/PIP finger bend, palm arch and thumb cross sensors included in the PCA and cluster analyses, we performed graph analysis with GraphVar (Release V2.01) [35] as implemented in Matlab. Restricting to runs for which PC1 was assigned to the associated cluster, the analysis required first calculation of the 12 × 12 Pearson correlation matrices for 98 runs of the right hand and 105 of the left hand. From these were calculated mean matrices yielding a weighted undirected graph with 12 nodes and 66 edges for each hand. Negative weights, corresponding to negative correlations, were retained. To investigate subnetworks, the graphs were thresholded in steps of 0.05 for positive and negative weights. Global efficiencies for both graphs were calculated without thresholds. A null model network consisting of 100 random fully connected weighted graphs generated with 1000 iterations served as basis for comparison using the Mann-Whitney-U-Test. Finally, the graphs were submitted to the Louvain community detection algorithm [36] s implemented in the brain connectivity toolbox [37] using a gamma of one in order to determine the modularity of the graphs.
Temporal evolution of finger movements in space

To complement the group PCA and temporal analysis of individual sensors and underpin their understanding, we acquired 3D data for male subject ID 10 in an additional acquisition. The group cluster analysis showed that PC1 of the subject had been assigned to the corresponding cluster in all runs of the right and in most runs of the left hand (Figs. 2, Fig S2). Software provided by Virtual Realities converts the raw sensor data into the C3D file format (www.c3d.org) used in biomechanics, animations and gait analysis laboratories. This format comprises 23 data points representing a standardized 3D hand model, each consisting of x, y, and z values in millimeters. Because the finger tips play a central role in the task, we focused on the five data points representing the end of the distal phalanges to calculate spatial finger trajectories and average speed. A trajectory was defined as the points between consecutive maximal extensions of the thumb derived from repeated manipulations, as determined by the program findpeaks of Matlab.

As in group acquisitions, the data were acquired as 6 runs of 16 sec each. However, the sampling rate was 36.97 Hz, the prescribed rate for the 3D acquisition mode. Since the time between maximum extensions of the thumb varied, the number of trajectories was less than optimum: 80 for the right hand and 75 for the left. The speed of finger movement were then computed by dividing the path length of the trajectory by its duration. From the ensemble of trajectories for each hand were calculated a mean trajectory and 95% CL (confidence level) region, the latter using an error ellipsoid for each time point with the Matlab program error ellipse (https://ch.mathworks.com/matlabcentral/fileexchange/4705-error_ellipse). For visualization, the trajectories of approximately 37 frames were resampled to 100 frames and the mean trajectories and CL region displayed (Video 1) using the open source software Mokka version 0.6.2 (https://biomechanical-toolkit.github.io/mokka/).

Results

Sensori-motor assessment

The group tested normal in the sensori-motor assessment of functional tactile exploration. As indicated in Table S1 in Supporting Information, this result agrees with published data regarding age- and gender-matched healthy controls for power and precision grip [26], PSO [38], two point discrimination and TOR [28].

Spatial sensor pattern

An initial PCA of the time series was performed for all 29 glove sensors for left and right hand of all runs and subjects. These analyses showed that 10 sensors, including the 8 sensors comprising the hand and wrist quaternion, and the pressures sensors P4 and P5 only marginally involved in the task as related to object size, yielded small expression coefficients. The nineteen sensors reflecting specifically prehensile in-hand manipulation as postulated in the introduction produced expression coefficients consistently within a 90% confidence interval (CI) range ($0.05 < p < 0.95$): all ten finger bend sensors, all four ab/adduction sensors, three pressure sensors related to thumb as well as index and middle finger pads (P1 – P3) previously shown predominantly involved in this manipulation task (8), and two sensors describing the deformation of the palm: palm arch and thumb cross. These relevant sensors were submitted to further analysis.

A PCA of each of the six runs for each subject yielded a total of 132 analyses for each hand. The Guttman-Kaiser criteria (GK) for salient PCs yielded a mean value computed for all PCAs of 3.73 ± 0.84 for the left hand and 3.95 ± 0.82 for the right. Since the first three PCs of each run yielded mean fractions of variance explained of 81% ± 6% for the left hand and 78% ± 6% for the right, further analysis was restricted to these first three PCs. Not unexpectedly, a significant negative correlation emerged between the fraction of variance explained by PC1 and the GK criteria (left and right $p < 2 \times 10^{-14}$) and a significant positive correlation between that explained by PC3 and the GK criteria (left and right $p < 1 \times 10^{-11}$).

After the realignment described in Methods, the expression coefficients of the first three PCs of all subjects and runs, i.e. $3 \times 132 = 396$ sets of expression coefficients for each hand, were assigned to one of three clusters according to K-means clustering as described above. As shown in Fig. 2, 98 PC1's were assigned to Cluster1 of the right hand and 105 PC1's to Cluster1 of the left. The Fisher's exact test indicated no significant difference between hands regarding the number of assignments. The numbers of PC2 assigned to Cluster 2 were 82 for the right hand and 102 for the left; they differ significantly at level, $p < 0.01$. Finally, as shown in Figure S1 of the Supporting Information, the numbers of PC3 assigned to Cluster3 were 74 for the right hand and 91 for the left; they differ significantly at level, $p < 0.05$. Further comparison of Cluster1's reveals that the means and confidence intervals of the correctly assigned PCs are comparable, but that the spread of distances for the misassigned PC1's is markedly greater in Cluster1 of the right hand. Both the means and confidence intervals of the Cluster2's and Cluster3's are greater than those of the Cluster1's for both hands. Thus, the left hand appears to show a clearer pattern of PC assignments to clusters. Regarding misassignments, 32 of 34 of the misassigned PC1's of Cluster1

are assigned to Cluster2 for the right hand; 20 of the 27 misassigned PC1's of Cluster1 are assigned to Cluster2 for the left hand. The difference indicates a trend: $p < 0.07$. Furthermore, 41 of 58 missassigned PC3s of the right hand and 27 of 43 PC3's of the left hand are assigned to their respective Cluster2's, suggesting a mutability between the two, although the centroids are not significantly correlated; $p < 0.14$ for the right hand and $p < 0.19$ for the left.

The mean spatial trajectories related to the end phalanges and joint sensors are shown in the animation calculated for subject ID10, based on the glove data and compiled in the C3D file format (Video 1). An expression coefficient related to a specific sensor expresses only the relative extent of movement in the main plane of a joint (flexion and adduction for positive and extension and abduction for negative values), or local pressure (less pressure for positive and more pressure for negative values) in a particular component, which represents a phase of the trajectory. Figure 3 shows the expression of the glove sensors related to the joints in the Clusters 1 and 2 for right and left hands. To focus on movement pattern (i.e. the major aim of the study) subtle finger pad pressure changes are not featured in Figure 3 but qualitatively described below and integrated in the Figure SF3 of Supporting Information. An omnibus Kruskal Wallis analysis of the correctly assigned expression coefficients indicated in red and summarized in Table 2 showed clearer inhomogeneities among the sensor patterns than the means and cluster centroids indicated in blue and black, at $p<<e-10$ for PC1-3 on both sides. The patterns of the Cluster1's show prominence of thumb cross and palm arch sensors, indicating movement of the carpometacarpal joint (CMC) of the thumb in both hands. In the right hand, the PIP joints of all fingers and increased thumb pressure are out of phase; in the left, the MCP joints of the fingers and thumb abduction are in phase with the thumb CMC whereas the PIP joints are out of phase together with increased thumb pressure. The parameters of the Cluster2's reveal in the right hand simultaneous activation of the PIP and MCP joints of the fingers, abduction between index and middle finger and between middle and ring finger, reduced pressure of thumb are also in phase; out of phase are all thumb joints as well as abduction between thumb and index finger. In the left hand, activation of the PIP joints of all fingers accompanies diminished pressure of the thumb; thumb cross (CMC) and palm arch sensors are out of phase as are abduction between index and middle, middle and ring and ring and little fingers and flexion of the little and middle MCP fingers. The sensor patterns of Cluster3's (shown in Supporting Information SF3) provided little additional information related to finger interplay. Thumb pressure in the right hand accompanies simultaneous flexion of middle, ring and little finger MCP joints; the pattern of prominent thumb cross and palm arch in the left hand is similar to Cluster 1 of the right hand. Post-hoc multiple comparison test using the multicompare matlab program of the ranks validated the salience of three groups of sensors: thumb cross with palm arch as well as MCP and PIP joints of the fingers exhibited highly significant variations due to phase differences between changing thumb to finger oppositions, satisfying a p-value of <0.05 after correction for multiple comparisons according to Bonferroni.

Table 2. Non-parametric tests of prominent bend sensor expression coefficients and post-hoc pairwise analysis.

Kruskal Wallis	PC1 lt	P = 2.98e-204	Pos. EC		Neg. EC	PC1 rt	p = 2.50e-121	Pos. EC		Neg. EC
Multicompare			MCP (I, M, R, L)	vs *	PIP (I, M, R, L), PArch			Tcross, PArch	vs *	MCP (I, M, R, L)
			Tcross		PIP (I, M, R, L)			Tcross, PArch		PIP (I, M, R, L)
Kruskal Wallis	PC2 lt	P = 5.40e-153	Pos. EC		Neg. EC	PC2 rt	p = 5.72e-62	Pos. EC		Neg. EC
Multicompare			PIP (I, M, R, L)	vs *	MCP (I, M, R, L)			MCP (I, M, R, L)	vs *	Tcross, PArch
			PIP (I, M, R, L)		Tcross			PIP (R)		Tcross
			PIP (I, M, R, L)		PArch			PIP (M, R, L)		PArch
Kruskal Wallis	PC3 lt	P = 7.73e-65	Pos. EC		Neg. EC	PC3 rt	p = 2.90e-37	Pos. EC		Neg. EC
Multicompare			Tcross	vs *	MCP (I, M, R, L), PIP (I)			PIP (L)	vs *	MCP (M, R, L)
			PArch		MCP (M, R, L)					

Kruskal Wallis and Multicompare analysis implemented in Matlab.

* All shown differences for post-hoc Multicompare are significant at $p < 0.05$ after correction for 19 comparisons according to Bonferroni.

Abbreviations: PC, Principal component; EC, expression coefficient; Rt, Right; Lt, Left; MCP, Metacarpo-phalangeal joints (I, Index; M, Middle; R, Ring; L, Little); PIP, Proximal interphalangeal joints (I, M, R, L); Tcross, Thumb cross sensor related to carpo-metacarpal joint of thumb; PArch, Palm Arch.

Temporal sensor patterns

We present below two types of temporal analysis in order to compare the motion of right and left hands: analyses 1) of the principal component time series and 2) of the complete time series of the three groups of sensors suggested by the spatial sensor patterns. The mean frequency spectra of the dominant PCs shown in Fig. 4 are very similar for the two hands. Determined mainly by the task instructions, the spectra peak at about 1 Hz; the spectra of PC1 showed a peak at 1.03 Hz for the right hand and at 1.07 Hz for the left. For PC2, the spectra showed peaks at 1.03 Hz and 0.93 Hz, respectively. A shoulder in both PCs at 2 Hz is more apparent for the right hand. The shoulder at lowest frequencies reflects a slow drift unrelated to the manipulation.

The negative and positive time delays between PCs shown in Fig. 4B confirm the independence observed in the spatial patterns. Almost all delays between PC1 and PC2 occur within a time window of 1 sec, i.e. 50 frames: 98% for the right hand and 90% for the left. The difference is marginally significant: $p < 0.05$, two-tailed. Moreover, the asymmetries of the delay distributions differ between hands and the differences are significant at the level, $p < 0.000$. The distributions of delays between PC1 and PC3 within the same time window are broader: 74% for the right hand and 70% for the left, which is not significantly different. To facilitate comparison of all delay distributions, Figure S4 displays them for a time window of 2 sec, i.e 100 frames.

Analysis of the complete time series of the three groups, comprising ten finger bend, palm arch and thumb cross sensors, is summarized in Table 3. It reveals no significant frequency differences between respective finger groups of the left and right hands nor among the three groups of each hand. All groups reproduce the instructed frequency within statistical deviations.

Sensor groups	Left hand (n = 105 runs)		Right hand (n = 98 runs)		p-value left vs right (Mann-Whitney-U-Test)
	mean	± SD	mean	± SD	
Thumb (4 sensors, incl. Palm Arch)	1.01	0.10	1.04	0.13	0.20
MCP (4 sensors)	1.01	0.13	1.01	0.12	0.98
PIP (4 sensors)	1.01	0.11	1.02	0.13	0.17
p-value Friedman's Test within one hand (thumb, MCP, PIP)	0.78		0.17		

Table 3. Comparison of frequencies for dominant groups of finger sensors. Of the the 19 relevant sensors, the 12 most prominent sensors are grouped as Thumb (IP, MCP, Thumb Cross and Palm Arch), MCP (of fingers) and PIP (of fingers) sensors.

Graph analysis of selected sensor time series

The time series of the 12 MCP/PIP finger bend, palm arch and thumb cross sensors included in the PCA and cluster analyses resulted in a weighted, undirected network for each hand. The number of positive weights: 29 of 66 edges or 43.9%, and negative weights: 37 of 66 edges or 56.1%, was equal in both hands. The edges with the highest positive weights connect the ring MCP and ring PIP (0.869) of the left hand and the ring PIP and little PIP (0.854) of the right hand. The edges with the lowest negative weights connect the thumb MCP and ring MCP (-0.421) of the left hand and the thumb MCP and little MCP (-0.503) of the right hand.

The networks of positive weights shown in Fig. 5, thresholded at 0.35 for better illustration, reveal three strongly connected sub-networks in each hand and three modules. One network in blue connects all MCP joints and another in green all PIP joints; these joints comprise also two of the modules. A third sub-network and module in red features a strong connection between palm-arch and thumb cross. The two isolated nodes of the right hand, thumb MCP and PIP, are members of the third module, whereas the thumb PIP joint of the left hand is a member of the PIP module. The networks of negative weights shown in Fig. 5, thresholded at -0.35 for better illustration, manifest the same modular structure as the positive weights, but the connections are intermodular. In the right hand, the connections between palm arch and index PIP and between thumb MCP and middle MCP are particularly strong; less strong are the connections between thumb CMC and ring and middle PIP, between thumb MCP, little MCP and index PIP, and between thumb PIP, middle and index MCP and index PIP.

Despite the differences between left- and right-hand networks suggested by Fig. 5, the global efficiencies and small world properties of the networks do not differ significantly. The mean global efficiencies of the

unthresholded networks were 0.95 ± 0.03 for the left and 0.94 ± 0.02 for the right hand, indicating no significant difference: $p < 0.11$. The mean small-world propensities, ϕ, were 0.53 ± 0.20 for the left and 0.49 ± 0.21 for the right hand, implying no significant difference: $p < 0.11$. The mean small-world indices, σ, were 1.39 ± 0.59 for the left and 1.45 ± 0.55 for the right hand, implying again no significant difference: $p < 0.12$. These values indicate that both networks show small-world properties, implying substantial clustering and small path lengths.

Temporal evolution of finger movements in space

To illustrate the spatial finger trajectories recorded during the special acquisition of 3D data for subject ID10, we focused on the five sensors located at the ends of the distal phalanges, i.e. P1-5. The trajectories depicted in Fig. 6A are repeated at median frequencies of 0.78 Hz by the left hand and 0.83 Hz by the right with interquartile ranges of 0.68–0.95 Hz and 0.75–0.92 Hz, respectively. These are slightly less than the frequencies measured by the twelve sensors that dominate the spatial sensor patterns of the subject cohort. The slightly slower repetition frequencies of the left hand accompany shorter trajectories and slower finger speeds than those of the right hand. As shown in the Supporting Information (Fig S5, Table S2), the middle finger tip of the left hand and the thumb tip of the right hand were the fastest with median speeds: 22 cm/s and 32 cm/s, respectively. The middle finger tip of the right hand showed the second fastest speed for that hand, 19 cm/s, only slightly faster than the ring finger tip, whereas the thumb tip of the left hand yielded the second slowest speed for that hand, 15 cm/s.

Discussion

The goal of our study was a spatial and temporal description in healthy volunteers of the dynamic finger movements involved in the brief manipulation of an elementary object, a cuboid. Subjects were instructed to handle the object at a frequency of 1 Hz to insure adequate task performance, a frequency sufficiently less than the 2 Hz at which completing the task becomes an issue [39, 40]. In order to facilitate adequate performance of this basic sensori-motor task, study participants were instructed to replicate the consecutive handling of a cuboid shown in a video immediately preceding execution. The video, showing repeated manipulations for a duration of 20 s at a frequency of 1 Hz, provided spatial and temporal cues for the finger movements prior to execution, and thus supported pre-attentive sensory processes whereas execution is based on proprioception [40, 41]. Thus, visual guidance provided by the video implied right hand/left hemisphere dominance rather than the left hand/right hemisphere associated with haptic guidance [42]. Our study cohort included only right-handed healthy volunteers whose ages matched those of stroke survivors to get a control group for recovery (Table 1).

Derived from the 19-dimensional glove sensor space, the first three PCs of each run explained 75 to 80 percent of the variance, and were thus salient according to the Gutmann Kaiser criterion [33]. This low dimensionality is consistent with the observations of Belic and Faisal; [22], Jarassé et al. [43] and Ingram et al. [44], who found that a few PCs explained a comparable percentage of total variance in tasks involving motor control of daily reach-to-grasp activities, bilateral hand movements and of natural,

spontaneously generated hand movements, respectively. The three PCs reflect a modular partition of motor synergies (see below) as also found in TMS experiments by Gentner and Classen [45].

In contrast to previous studies reporting finger trajectories in single reach-to-grasp tasks, in everyday activities [21–23, 43, 46] and in pure grasping tasks involving intrinsic hand movements [20, 47], we explored a sequence of defined manipulations of an almost regular cuboid embedded in the short action represented in Fig. 1C. From a hand-centric view, we have shown that the sequential handling can be partitioned into repeated motor acts involving partially independently moving fingers (44). During these acts the fingers interact with the object using so-called transitive movements in a workspace tightly adapted to the objects [48] as shown in Fig. 6. These movements are accompanied by motion of the object, which requires at least two fingers to hold the object while the perpendicular finger positions it (32). During this interaction occurs a continual change of finger configurations directed to contacts at the edges and vertices of the object (Li, Canny et Sastry, 1989) while the fingers in contact are replaced by free fingers once they have reached joint limits of a finger pair [15]. Thus the precise handling observed is prehensile motion within the contacting hand (see taxonomy in 32), suggesting the finger gaiting discussed below. In contrast to the hand-centric view, the object-centric view postulates that perceived attributes of the object may evoke motor acts during pure manipulation equivalent to those during active touch, i.e. stresses the aspect of the hand as sense organ (46). An analysis of natural hand movements confirmed the similarity of finger joint trajectories in both classes of prehensile in-hand activity (47).

In our study, the first principal component for both hands accounted typically for one half or more of the variance explained by the salient components. K-mean clustering provided a more detailed analysis of the subjects' cohort. The number of PC1's assigned to corresponding Cluster1's was comparable for both hands, 98 and 105 of the 132 runs for the right and left hands, respectively. The other two PCs showed significant differences between hands, as indicated in Figs. 2 and S1 of the Supporting Information. A greater number of PCs, 102 were correctly assigned to the corresponding clusters for the left hand compared to 82 for the right. The more flexible strategy of the right hand is indicated by the observation that the majority misassigned PC2's in Cluster 2 were assigned to Cluster 3 and vice versa. In the context of stochastic optimal feedback control proposed by Todorov and Jordan [49], these two mutable PCs might represent variability in task-irrelevant dimensions, and reflect fluent action in the dynamic activity of the right hand without exceeding normal limits. If task-irrelevant is substituted for salient, these observations are consistent with the observations of Faisal et al. [50], who found in archaeological toolmaking a correlation between the complexity of an underlying hand motor task and the number of salient components.

Represented in Fig. 3, the spatial patterns exhibited by the salient PCs appear to be encoded mainly by twelve of the nineteen sensors. These twelve imply three groups of coordinated and synergistic finger movements: a 1st group related to the carpo-metacarpal joint of the thumb together with palm arch sensor; a 2nd group related to the metacarpophalangeal (MCP) joints of the fingers; and a 3rd group related to the proximal interphalangeal (PIP) joints of the fingers. Trajectories associated with these joints have been shown to be stereotypical and characterized by multicollinearity of the MCP and PIP joints [8].

The Kruskal Wallis nonparametric analysis of the expression coefficient distributions established varying interactions among thumb and fingers, i.e. the opposition of the CMC (carpo-metacarpal) joint of the thumb and flexion of MCP and PIP joints, during the phases of the task performance represented by the principal components. These phases consist presumably of different grasp configurations composing the motor act demanded by the task, since the principal components exhibited a task frequency of 1 Hz and distinct short delays among them (Fig. 4B). The appearance of 2 to 3 configurations within 1 second confirms finger gaiting as principal mechanism underlying one motor act, which prevents loss of the cuboid [30]. This is the first time that finger gaiting is observed in a human sensori-motor task which is fundamental to the haptic exploration of objects, e.g. for shape perception, during which the fingers hold the object while it is surveyed by the thumb [51, 52].

The differences between right and left hands shown by the cluster analysis represent a new and important finding. In fact, Häger-Ross and Schieber [53] found evidence for individuation of the left thumb during cyclical flection and extensions of an opposing finger. However, they studied individuation at self-paced finger frequencies of 2 Hz and externally paced finger frequencies of 3 Hz where range control begins to override task pursuit control [39, 49]. We propose here that differentiation of the right thumb constitutes the foundation for performing with high accuracy the dynamic flection and rotation in the carpo-metacarpal joint necessary for fast finger opposition. The almost identical expressions of right palmar arch and thumb cross sensors in Clusters 1 and 2 may indicate synchrony between right thumb and shaping the hand during precise opposition to fingers, supporting the thumb's trajectories [29, 54]. The functional difference between the right and left thumb is an example of the reduction of hand degrees of freedom through introduction of a postural synergy at the right palmar arch [55].

Regarding the time series associated with the salient PCs, the frequency spectra shown in Fig. 4 evidence a clear peak at 1 Hz, the frequency of the repeated cuboid manipulations shown in the video immediately prior to execution of the task. This verifies the determining effect of an imitative cue in the time domain, analogue to the observation of Brass et al. [56] in the spatial domain. The time delays between the dominant and subdominant PCs for both hands confirm their independence. They are of both signs, but are significantly asymmetric with the dominant sign differing according to hand. Thus, no unique temporal sequence can be assigned to the spatial patterns.

The time series of the 12 sensors comprising three groups posited to engage in synergistic movements of the MCP and PIP joints of the fingers and the carpo-metacarpal joint of the thumb and palm arch also yielded median frequencies of 1 Hz in both hands. As suggested in Table 3, the frequencies of the fingers are consistent and homogenous for the three groups in each hand, suggesting an intrinsic harmonic, synchronous organisation (cf. 50,51).

Complementary analysis of the time series of the 12 sensors using graph theory provide new insights depicted in Fig. 5, establishing the modular organization of this multifinger task. It shows for the right hand positive correlations among analogous joints, MCP and PIP, of four fingers and between palm arch and thumb cross, and negative correlations among joints of arch and thumb and a majority of the finger

joints. The left hand shows similar, but fewer connections. The connections of the positively correlated nodes at the MCP and PIP joints may reflect repeated motor acts in the task and encode time varying motor information essential for a dynamical system engaged in manipulation [59]. The dense interconnections between MCP and PIP joints of adjacent fingers confirm the positive correlations between these joint pairs posited in the spatial patterns [60]. The connections of the negatively correlated nodes reflect anticorrelation between thumb and PIP and to a lesser degree MCP joints, compatible with their asynchrony among each other in the motor act patterns shown in Fig. 3. The graph analysis indicates high local movement efficiency and short paths among the interconnected joints, corroborating substantial global synchrony during the task within joint groups as detailed above [54, 61, 62]. The graphs of both hands exhibit small world characteristics and, most importantly, high global efficiency. Thus, the capacity for functional parallel synergy within the modules is equally great in both hands [63, 64].

The spatial finger trajectories shown in Fig. 6 illustrate for a single subject the temporal evolution of the finger tips in space. They represent the tangential sliding of the fingers as they encompass the cuboid. The paths are restricted, comprising only a small percentage of available workspace and limited degrees of freedom [55]. The workspace occupied by the trajectories of the right hand is much greater than that of the left hand, suggesting the greater variability associated with optimal feedback control [49] posited in the spatial patterns. The longer trajectories of the right hand imply that the speeds of the finger tips are greater [65], since the repetition frequencies are subordinated to the manipulation frequency of 1 Hz. The manifest differences between right and left hands observed in the spatial and temporal patterns of the PCA, in the graph analysis and in the trajectories of Fig. 6 may reflect the distinct roles of left and right hands in everyday human activities as reported in studies of bimanual tasks. In these tasks, the left hand provides rather stable postural support while the right assumes a more dynamic, spatially extended role [50, 66]. The variability of the right hand appears to be associated with a larger workspace as reflected by the mutability of assignments to the subordinate clusters.

Limitations are inherent in the choice of object to be explored and in precise instructions of how it should be explored. We relied deliberately on a theoretical model of human somatosensory exploration of kinesthesia developed and validated by Roland and Mortensen [67] in which information is sampled successively and sequentially. Hence, the application of this well-studied task allows generalization specifically to recognition of macroscopical aspects of objects, e.g. shape, as has been shown in a recent study by Abela et al. [28]. Moreover, multiple precision grips of the involved fingers during a sequence of consecutive manipulations are subject to failure above a grasping frequency threshold of 2 Hz. The selection of a cuboid as object and exploration frequency of 1 Hz was made to provide a prototypical task for the study of the post-stroke recovery of coordinated hand motor skills in a clinical context and of significance for daily motor needs (cf. 61). A complete description of the spatial trajectories associated with the task was beyond the scope of this study. The PCA and cluster analysis permitted the decomposition of a dynamic task into salient phases characterized by distinct finger configurations and frequencies, yielding insight into the mutability of the phases and time delays between them. This analysis motivated further analysis of the complete time series of individual finger joints and graph

analysis, which confirmed our findings. Delineation of the common workspace of all subjects will be the focus of a future study.

Conclusion

Using a digital data glove, we have exposed new spatial and temporal aspects of the object manipulation underlying tactile exploration. Most important, the task involved a series of hierarchically organized elementary grasp configurations, conjectured to be constituents of finger gaiting, which are incorporated in manipulation during precision handling. Three principal components proved to be adequate for both hands, confirming that their motor control is low-dimensional. Differences between right and left hands shown by the cluster analysis are striking. The related spatial patterns revealed a less variable resolution of the three principal components describing finger movements of the left hand than of the right hand, suggesting a less flexible strategy in the former and, thus, less dexterity. The greater variability of the right hand appears to be related to the larger proprioceptive motor space occupied by the movements, as illustrated by the analysis in a single subject of the temporal evolution in space. The differences are obvious especially in the function of the CMC joint of the thumb in opposition to the MCP and PIP joints of the remaining fingers. Whereas opposition of the thumb to the MCP and PIP joints appears to be the dominant feature of manipulations with the right hand, synchronous movements in the MCP joints with the thumb as related to the CMC joint appears to be the dominant feature with the left hand, while the PIP joints are out of phase. The interactions among the three groups of thumb, MCP and PIP joints were further established by graph and frequency analysis of their synergistic movements. In addition to providing a prototypical task for the study of the post-stroke recovery, the sequence of basic manipulations required by the task might serve as a model of human tactile object recognition involving prehensile in-hand manipulation relevant also to the development of robotic tactile perception systems [5, 69, 70].

List Of Abbreviations

2PD: Two-point discrimination

CI: confidence interval

CL: confidence level

CMC: carpo-metacarpal joint

EC: expression coeffizient

FIR: finite impulse response

fMRI: functional magnetic resonance imaging

GK: Guttman-Kaiser criteria

IP: proximal interphalangeal joint

JTT: Jebsen-Taylor Test

KEK: Kantonale Ethikkommission Bern

LQ: laterality quotient

MCP: metacarpo-phalangeal joint

MMSE: Mini-Mental State Examination

PArch: Palm Arch sensor

PC: principal component

PCA: principal component analysis

PIP: Proximal interphalangeal joint

PSO: Picking Small Objects

SM1: primary sensori-motor

Tcross: thumb cross sensor

TOR: tactile object recognition

Declarations

Ethics approval and consent to participate

The study received ethical approval from the Kantonale Ethikkommission Bern (KEK), 3010 Bern, Switzerland (study number 2016-00417). Prior to the study all participants gave written informed consent before enrolment, according to the Declaration of Helsinki.

Consent for publication

Not applicable.

Availability of data and materials

The datasets generated during the current study and study protocol are available in the Open Science Framework (OSF) repository at https://osf.io/jp825/ .

Competing interests

No competing interests to declare.

Funding

This work was supported by the Swiss National Science Foundation (SNF Grant number 160107, www.snf.ch), the Swiss Heart Foundation (https://www.swissheart.ch) and the Clinical Trials Unit at the Cantonal Hospital of St.Gallen, Switzerland.

The funders had no role in study design, data collection and analysis, decision to publish, or preparation of the manuscript.

Authors' contributions

Concept and design: JHM,RW,BJW

Acquisition, analysis, or interpretation of data: WK,JHM,SH,BJW

Critical revision of the manuscript for important intellectual content: WK,JHM, MP-W,RW,BJW

Statistical analysis: WK,JHM,BJW

Administrative, technical, or material support: WK,SH,MP-W

Obtained funding: WK,MP-W,RW,BJW

Supervision: JHM,MP-W,BJW

Acknowledgements

We are grateful to our normal volunteers for supporting our research.

References

1. Ekstrand E, Rylander L, Lexell J, Brogårdh C (2016) Perceived ability to perform daily hand activities after stroke and associated factors: a cross-sectional study. BMC Neurol 16:208
2. Térémetz M, Colle F, Hamdoun S, Maier MA, Lindberg PG (2015) A novel method for the quantification of key components of manual dexterity after stroke. J Neuroeng Rehabil 12:64
3. Jones LA, Lederman SJ (2006) Human Hand Function. https://doi.org/10.1093/acprof:oso/9780195173154.001.0001
4. Li Z, Canny JF, Sastry SS (1989) On motion planning for dexterous manipulation. I. The problem formulation. https://doi.org/10.1109/robot.1989.100078
5. Bicchi A (2000) Hands for Dexterous Manipulation and Powerful Grasping: A Difficult Road Towards Simplicity. Robot Res 16:652–662

6. Piitulainen H, Bourguignon M, De Tiège X, Hari R, Jousmäki V (2013) Corticokinematic coherence during active and passive finger movements. Neuroscience 238:361–370
7. Pailiard J (1991) Motor and representational framing of space. 182:163–182
8. Kamper DG, Cruz EG, Siegel MP (2003) Stereotypical Fingertip Trajectories During Grasp. J Neurophysiol 90:3702–3710
9. Roland PE, Mortensen E (1987) Somatosensory detection of microgeometry, macrogeometry and kinesthesia in man. Brain Res Rev 12:1–42
10. Hartmann S, Missimer JH, Stoeckel C, Abela E, Shah J, Seitz RJ, Weder BJ (2008) Functional connectivity in tactile object discrimination - A principal component analysis of an event related fMRI-study. PLoS One. https://doi.org/10.1371/journal.pone.0003831
11. Kägi G, Missimer JH, Abela E, Seitz RJ, Weder BJ (2010) Neural networks engaged in tactile object manipulation: Patterns of expression among healthy individuals. Behav Brain Funct 6:71
12. Seitz RJ, Roland PE, Bohm C, Greitz T, Stone-Elander S (1991) Somatosensory Discrimination of Shape: Tactile Exploration and Cerebral Activation. Eur J Neurosci 3:481–492
13. Stoeckel MC, Weder B, Binkofski F, Buccino G, Shah NJ, Seitz RJ (2003) A fronto-parietal circuit for tactile object discrimination: An event-related fMRI study. Neuroimage 19:1103–1114
14. Weisstanner C, Kägi G, Krammer W, Eap CB, Wiest R, Missimer JH, Weder BJ (2018) The effect of a single dose of escitalopram on sensorimotor networks. Brain Behav 8:e00975
15. Han L, Trinkle JC (1998) Dextrous manipulation by rolling and finger gaiting. In: Proc. - IEEE Int. Conf. Robot. Autom. pp 730–735
16. Fan Y, Gao W, Chen W, Tomizuka M (2017) Real-Time Finger Gaits Planning for Dexterous Manipulation. IFAC-PapersOnLine. https://doi.org/10.1016/j.ifacol.2017.08.1831
17. Landsmeer JM (1962) Power grip and precision handling. Ann Rheum Dis 21:164–170
18. Castiello U (2005) The neuroscience of grasping. Nat Rev Neurosci 6:726–736
19. Cutkosky MR (1989) On grasp choice, grasp models, and the design of hands for manufacturing tasks. IEEE Trans Robot Autom 5:269–279
20. Feix T, Romero J, Schmiedmayer H-B, Dollar AM, Kragic D (2016) The grasp taxonomy of human grasp types. IEEE Trans Human-Machine Syst 46:66–77
21. Santello M, Flanders M, Soechting JF (1998) Postural hand synergies for tool use. J Neurosci 18:10105–15
22. Belic JJ, Faisal AA (2015) Decoding of human hand actions to handle missing limbs in neuroprosthetics. Front Comput Neurosci 9:27
23. Thakur PH, Bastian AJ, Hsiao SS (2008) Multidigit Movement Synergies of the Human Hand in an Unconstrained Haptic Exploration Task. J Neurosci 28:1271–1281
24. Oldfield RC (1971) The assessment and analysis of handedness: the Edinburgh inventory. Neuropsychologia 9:97–113

25. World Medical Association (2013) World medical association declaration of Helsinki. Japanese Pharmacol Ther 28:983–986
26. Mathiowetz V (1985) Grip and Pinch Strength: Normative Data for Adults. Arch Phys Med Rehabil 66:69–72
27. Tong J, Mao O, Goldreich D (2013) Two-Point Orientation Discrimination Versus the Traditional Two-Point Test for Tactile Spatial Acuity Assessment. Front Hum Neurosci. https://doi.org/10.3389/fnhum.2013.00579
28. Abela E, Missimer JH, Pastore-Wapp M, Krammer W, Wiest R, Weder BJ (2019) Early prediction of long-term tactile object recognition performance after sensorimotor stroke. Cortex 115:264–279
29. Hertling D, Kessler RM (1996) Management of common musculoskeletal disorders : physical therapy principles and methods. https://doi.org/10.1097/00003465-199009000-00008
30. Bullock IM, Ma RR, Dollar AM (2013) A hand-centric classification of human and robot dexterous manipulation. IEEE Trans Haptics 6:129–144
31. Varela J V, Toro A, John ER, Schwartz (1981) Perceptual framing and cortical alpha rhythm. Neuropsychologia 19:675–686
32. Alexander GE, Moeller JR (1994) Application of the scaled subprofile model to functional imaging in neuropsychiatric disorders: A principal component approach to modeling brain function in disease. Hum Brain Mapp 2:79–94
33. Guttman L (1954) Some necessary conditions for common-factor analysis. Psychometrika 19:149–161
34. Bro R, Leardi R, Johnsen LG (2013) Solving the sign indeterminacy for multiway models. J Chemom 27:70–75
35. Kruschwitz JD, List D, Waller L, Rubinov M, Walter H (2015) GraphVar: a user-friendly toolbox for comprehensive graph analyses of functional brain connectivity. J Neurosci Methods 245:107–115
36. Blondel VD, Guillaume J-L, Lambiotte R, Lefebvre E (2008) Fast unfolding of communities in large networks. J Stat Mech Theory Exp 2008:P10008
37. Rubinov M, Sporns O (2010) Complex network measures of brain connectivity: Uses and interpretations. Neuroimage 52:1059–1069
38. Jebsen RH, Taylor N, Trieschmann RB, Trotter MJ, Howard LA (1969) An objective and standardized test of hand function. Arch Phys Med Rehabil 50:311–9
39. Freund HJ (1986) Time control of hand movements. Prog Brain Res 64:287–294
40. Kunesch E, Binkofski F, Freund H-J (1989) Invariant temporal characteristics of manipulative hand movements. Exp Brain Res 78:539–546
41. Roland PE (1978) Sensory feedback to the cerebral cortex during voluntary movement in man. Behav Brain Sci 1:129–147
42. Stone KD, Gonzalez CLR (2015) The contributions of vision and haptics to reaching and grasping. Front Psychol 6:1403

43. Jarrassé N, Ribeiro AT, Sahbani A, Bachta W, Roby-Brami A (2014) Analysis of hand synergies in healthy subjects during bimanual manipulation of various objects. J Neuroeng Rehabil 11:113
44. Ingram JN, Körding KP, Howard IS, Wolpert DM (2008) The statistics of natural hand movements. Exp brain Res 188:223–236
45. Gentner R, Classen J (2006) Modular Organization of Finger Movements by the Human Central Nervous System. Neuron 52:731–742
46. Mason CR, Gomez JE, Ebner TJ (2001) Hand synergies during reach-to-grasp. J Neurophysiol 86:2896–2910
47. Smeets JBJ, Brenner E (1999) A new view on grasping. Motor Control 3:237–271
48. Binkofski F, Kunesch E, Classen J, Seitz RJ, Freund H-J (2001) Tactile apraxia: unimodal apractic disorder of tactile object exploration associated with parietal lobe lesions. Brain 124:132–144
49. Todorov E, Jordan MI (2002) Optimal feedback control as a theory of motor coordination. Nat Neurosci 5:1226
50. Faisal A, Stout D, Apel J, Bradley B (2010) The manipulative complexity of lower paleolithic stone toolmaking. PLoS One. https://doi.org/10.1371/journal.pone.0013718
51. Okamura AM, Turner ML, Cutkosky MR (1997) Haptic exploration of objects with rolling and sliding. pp 2485–2490
52. Hömke L, Amunts K, Bönig L, Fretz C, Binkofski F, Zilles K, Weder B (2009) Analysis of lesions in patients with unilateral tactile agnosia using cytoarchitectonic probabilistic maps. Hum Brain Mapp 30:1444–1456
53. Häger-Ross C, Schieber MH (2000) Quantifying the independence of human finger movements: comparisons of digits, hands, and movement frequencies. J Neurosci 20:8542–50
54. Schieber MH, Santello M (2004) Hand function: peripheral and central constraints on performance. J Appl Physiol 96:2293–2300
55. Bicchi A, Gabiccini M, Santello M (2011) Modelling natural and artificial hands with synergies. Philos Trans R Soc B Biol Sci 366:3153–3161
56. Brass M, Bekkering H, Wohlschläger A, Prinz W (2000) Compatibility between observed and executed finger movements: Comparing symbolic, spatial, and imitative cues. Brain Cogn 44:124–143
57. Mason CR, Gomez JE, Ebner TJ (2001) Hand synergies during reach-to-grasp. J Neurophysiol 86:2896–2910
58. Santello M, Flanders M, Soechting JF (2018) Patterns of Hand Motion during Grasping and the Influence of Sensory Guidance. J Neurosci 22:1426–1435
59. Berniker M, Kording KP (2015) Deep networks for motor control functions. Front Comput Neurosci. https://doi.org/10.3389/fncom.2015.00032
60. Santello M, Flanders M, Soechting JF (2002) Patterns of hand motion during grasping and the influence of sensory guidance. J Neurosci 22:1426–35
61. Bassett DS, Bullmore ET (2017) Small-World Brain Networks Revisited. Neuroscientist 23:499–516

62. Stam CJ, van Straaten ECW (2012) The organization of physiological brain networks. Clin Neurophysiol 123:1067–1087
63. Latora V, Marchiori M (2001) Efficient behavior of small-world networks. Phys Rev Lett 87:198701
64. van den Heuvel MP, Sporns O (2013) Network hubs in the human brain. Trends Cogn Sci 17:683–696
65. Smeets JBJ, Brenner E (2001) Independent movements of the digits in grasping. Exp Brain Res 139:92–100
66. Guiard Y (2013) Asymmetric Division of Labor in Human Skilled Bimanual Action. J Mot Behav 19:486–517
67. Roland PE, Mortensen E (1987) Somatosensory detection of microgeometry, macrogeometry and kinesthesia in man [published erratum appears in Brain Res 1987 May;434(2):241]. Brain Res Rev 12:1–42
68. Binkofski F, Kunesch E, Classen J, Seitz RJ, Freund HJ (2001) Tactile apraxia Unimodal apractic disorder of tactile object recognition associated with parietal lobe lesions, Brain, vol. 124, pp. 132–144, 2001. 1934:132–144
69. Kang SB, Ikeuchi K (1997) Toward automatic robot instruction from perception - Mapping human grasps to manipulator grasps. IEEE Trans Robot Autom 13:81–95
70. Dijkerman HC, de Haan EHF (2007) Somatosensory processes subserving perception and action. Behav Brain Sci 30:139–189

Video 1

Video 1. The video shows the mean spatial trajectories related to the tip of end phalanges as well as the vertex of the joint angles of finger and thumb sensors in individual ID10. The 3D dimensions of the trajectories correspond exactly to those of the workspace in Figure 6, which is related there to the thumb and finger tips. The video displays the succession of 10 manipulations in normal and three in slow motion. Note: The 3D-Model of the left and right hand are in different space related to the preferred subject's hand position on the desktop, however the x, y and z-axis have the same aspect ratios.

Figures

Figure 1

A) Labels of all sensors, B) representation of a hand in the data glove holding the cuboid, C) image sequence of instruction video showing manipulation of cuboid.

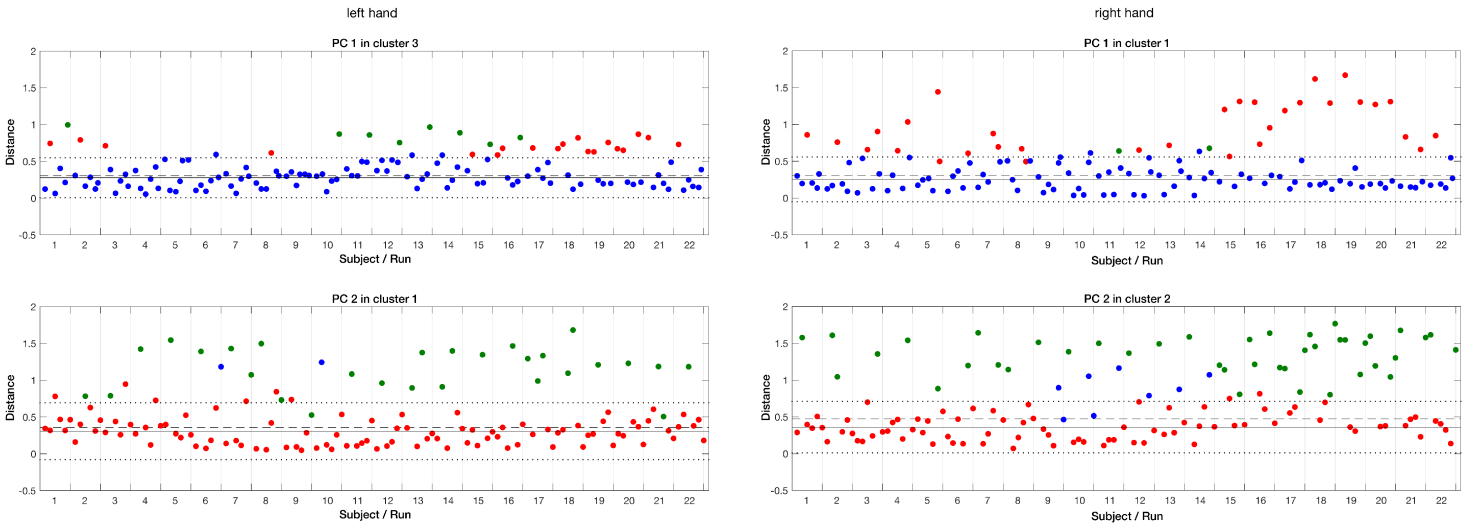

Figure 2

K-mean cluster classification of sensor patterns for PC1 and PC2 of left and right hands. The clusters are defined by the dominant PC, i.e. cluster 1 by PC1, cluster 2 by PC2 and cluster 3 by PC3 (Figure S2). The distances are derived from the correlation between the cluster centroid and the spatial pattern of a run. The colour blue denotes the PC1's, red the PC2's and green the PC3's. The medians, means, and 2 □ bands of the dominant PC's of a cluster are represented as dashed, solid and dotted lines, respectively. Misassigned runs are paled.

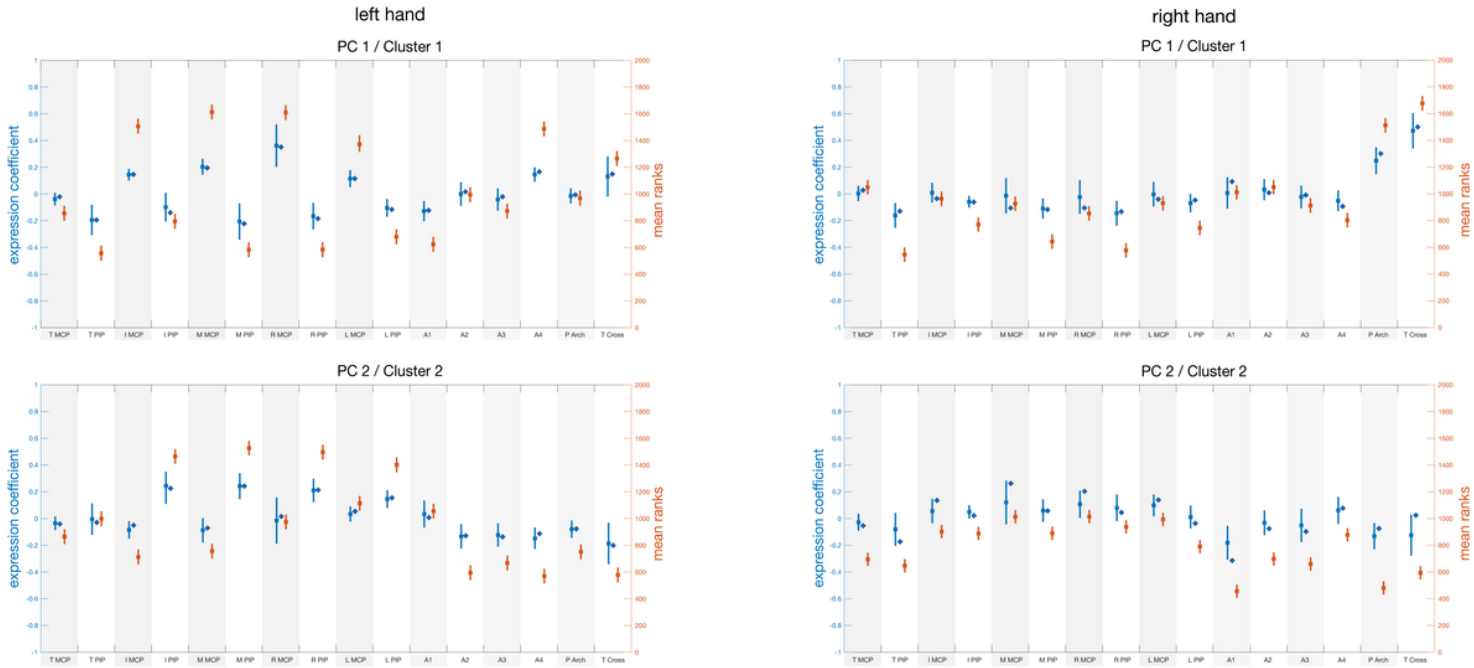

Figure 3

Spatial sensor patterns for PC1 and PC2 of left and right hands. The means and standard deviations of the expression coefficients determined for the dominant PCs in a cluster are represented by blue circles and bars. The adjacent diamonds denote the cluster centroids. The means and standard deviations of the

ranks according to the Kruskal-Wallis analysis are represented by red circles and bars. The y-axes are coloured correspondingly; the x-axes label the sensors as in Figure 1. A and Table 3.

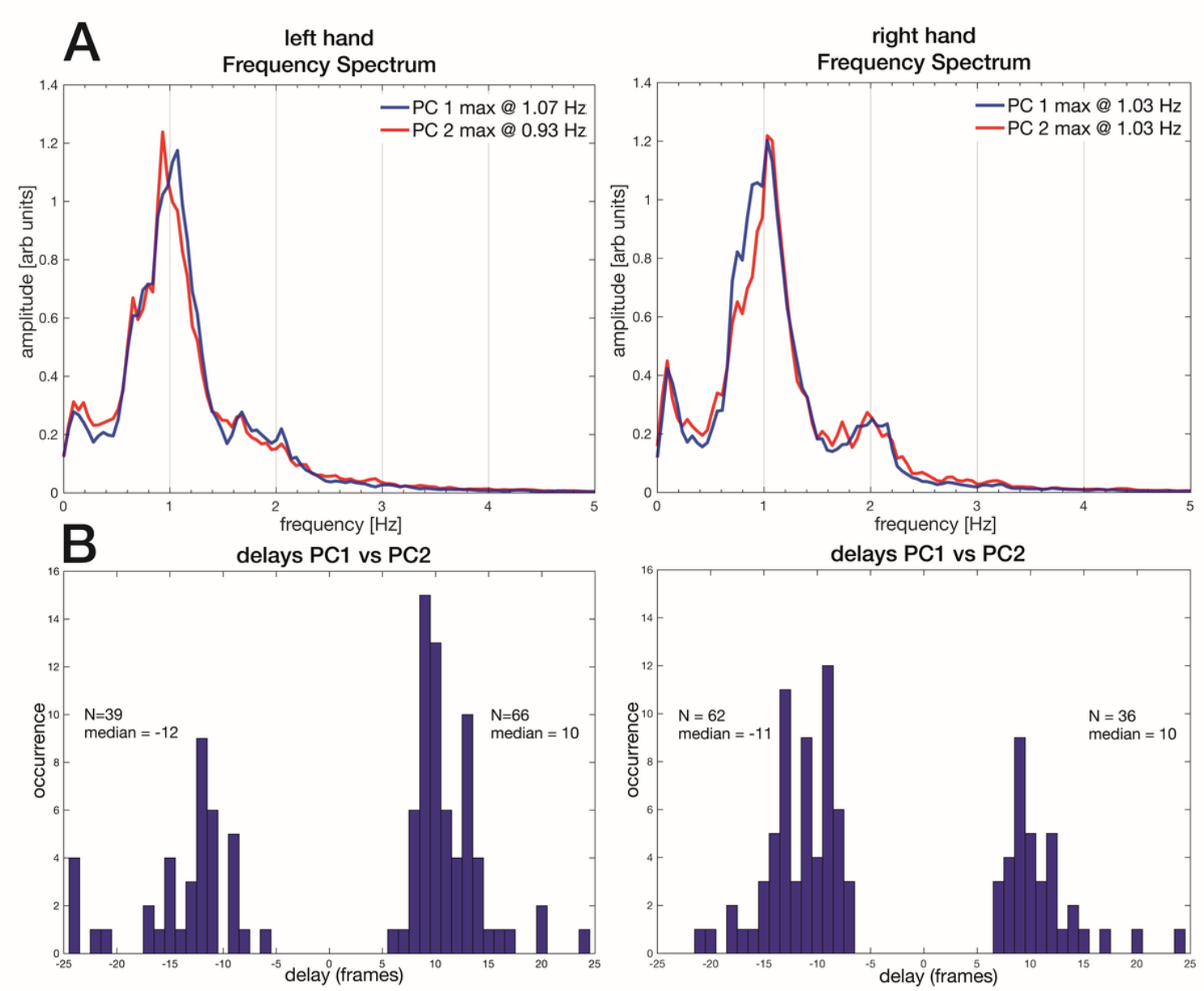

Figure 4

Temporal sensor frequencies and delays for PC1 and PC2 of left and right hands, calculated for dominant components of a cluster. A) Normalized frequency spectra in which blue denotes PC1 and red PC2, and B) histograms of the delays between PC1 and PC2 in frames (1 frame = 0.02 sec). Almost all the represented dominant components of PC1 and PC2 arise within 1 second manipulation corresponding to a related changing grasp configuration at that time window.

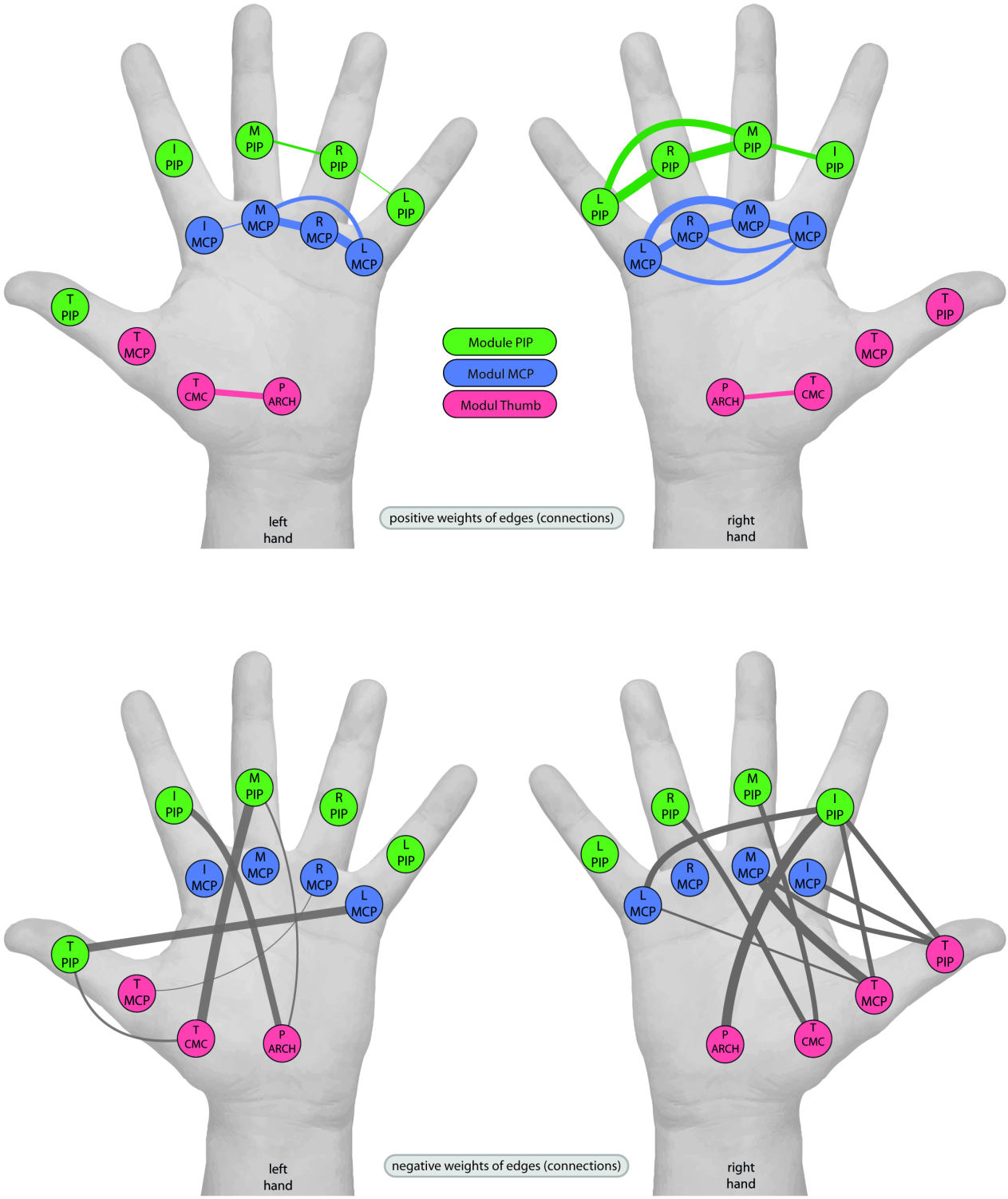

Figure 5

Pictorial representation of graph analysis for left and right hands as related to the mainly involved joints by the task, with positive weights in the upper row and negative weights in the lower row. Nodes' colour displays the modular structure in each hand, almost identical on the right and left. Nodes are denoted by their sensor labels, the relative weights of the connections indicated by the thickness of the lines between them (at a threshold of 0.35 in the upper row, and at a threshold of -0.35 in the lower row). Note the strong

intramodular connections in the positive weighted graph and the strong intermodular connections in the negative weighted graphs.

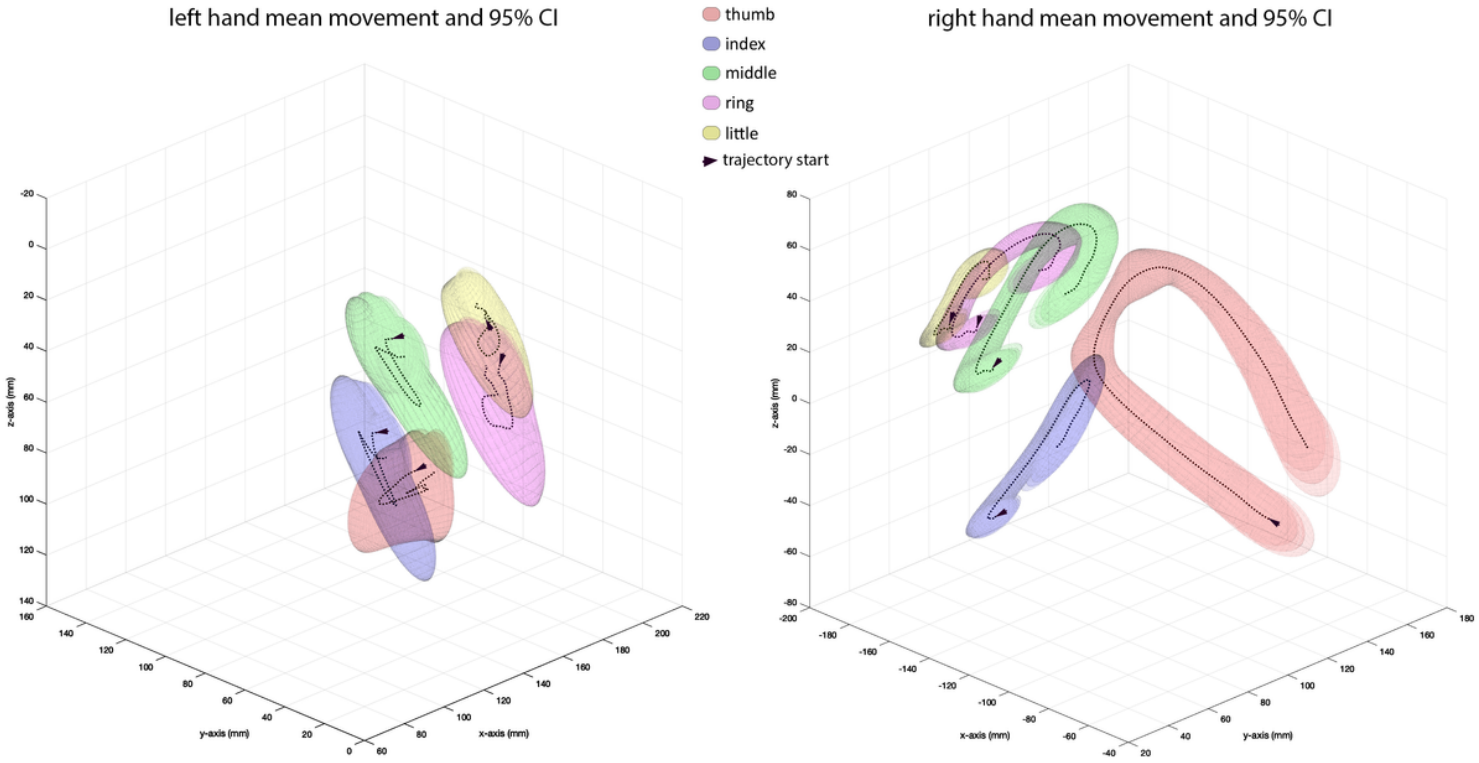

Figure 6

Finger trajectories in 3 dimensions for left and right hands derived from six runs of a single right-handed subject (ID 10). The black dotted lines indicate the mean position of the finger tip sensors, P1-5, and the colours the 2□ tubes of the trajectories. Note (1) the opposed position of the thumb to fingers on both sides, while the workspace is considerably restricted on the left compared to the right; and (2) the clockwise rotation of the spatial trajectories involving thumb and fingers on the right, and the anticlockwise rotation on the left.

Supplementary Files

This is a list of supplementary files associated with this preprint. Click to download.

- Video1.mp4
- FigS4.tif
- FigS3.tif
- FigS2.tif
- FigS1.tif
- SupportingInformationSensingform.docx